Effects of Power Supply Resonances in Onset Studies of Quasi-Steady MPD Thrusters

Luke Uribarri* and E. Y. Choueiri†

Electric Propulsion and Plasma Dynamics Laboratory, Princeton University, Princeton, NJ, 08544

A method for determining the extent to which power supply resonances alter measurements of onset voltage hash in MPD thrusters is presented. Such resonances can significantly distort the measured waveforms of voltage hash and can thus change the physical interpretations drawn from measurements. This artifice was likely present in many experimental onset studies. Lumped-parameter circuit analysis is used to model the resonance that arises in the transmission line connecting the power supply to the thruster. The resonance magnitude grows with increasing distance between the thruster and the voltage measurement. Experimental demonstration of the theoretically derived results is provided by a comparison of voltage hash measured near the thruster and at a point 1 m away, and by a measurement of the current using a novel Rogowski coil. It is shown that the power supply resonance produces a spurious dominant broadband frequency peak in the voltage hash power spectrum (in the present experiment, at 1.3 MHz), obscuring the physically meaningful hash waveform. The effect of the resonance on the current, however, is shown to be negligibly small, creating oscillations on the order of 1% of the quasisteady pulse value.

I. Introduction

The magnetoplasmadynamic thruster (MPDT) is an in-space plasma propulsion device that combines a high thrust density and high specific impulse (compared with, respectively, Hall thrusters and arcjets, for example), making it a viable candidate for such missions as Mars cargo transfer. Several issues remain to be resolved, however, before the MPDT can take on the role of main propulsion system on a flight vehicle. Perhaps the least understood of these is the "onset" problem.

Onset is the name used to denote the tendency of the MPDT to transition between two modes of operation as the current driving the arc is raised from low to high values. The low-current mode is characterized by a quiescent, low-level voltage and negligible erosion of the thruster anode (the thruster cathode is at all times subject to some degree of erosion). The high-current—onset—mode features, in contrast, a high-amplitude, fluctuating voltage (known as "hash") and significant anode erosion.

Attempts to understand the origin of onset fall into two categories: the prediction of the threshold current (which is not the focus of this paper), and the study of thruster behavior once the threshold is exceeded. In this second category, several researchers have found that the frequencies of oscillating parameters are roughly on the order of 100 kHz. Kuriki et. al.[7] measured such frequencies in the voltage hash and in all-light luminosity fluctuations in their quasisteady MPD thruster; Kurtz et. al[8] observed fluctuations in the 200–300 kHz range on a floating potential probe in a steady-state MPDT; Diamant et. al.[4] observed plasma density fluctuations with a Langmuir probe at approximately 100 kHz in the Princeton Benchmark thruster. In each of these cases, however, it is unclear to what extent the observed frequencies are due to thruster physics, rather than to natural resonances of the power supply system.

In our own investigation of onset phenomena in the Princeton Benchmark thruster, we have found that measurements of the most commonly measured fluctuating quantity—the thruster voltage—are easily corrupted by the influence of the thruster power supply if they are not taken carefully. In general, the MPDT literature has not been specific about reporting the details of voltage measurement procedures, making it

*Graduate Student, Mechanical and Aerospace Engineering

†Chief Scientist EPPDyL, Associate Professor Mechanical and Aerospace Engineering Department, choueiri@princeton.edu

difficult to determine to what extent the published voltage hash data are a reliable representation of thruster physics. In this paper, we detail a method for determining the extent to which power-supply effects on the measured voltage may be expected and provide experimental demonstration of the theoretically derived results. We also present a complementary current diagnostic, based on a Rogowski coil, designed to provide information on the thruster current behavior during periods in which the thruster voltage is fluctuating. With these diagnostics we demonstrate that interpretations of the thruster voltage can be significantly affected by the influence of the power supply, but that the effect on the current measurement is small enough to be neglected in onset analysis.

We begin in Sec. II by describing the specific MPDT system used in this paper. Section III describes the challenge of measuring a fluctuating voltage in an MPDT with a remote power system, first mathematically in Sec. III.A and then experimentally in Sec. III.B. We then go on to describe the MPDT current measurement in Sec. IV; again, we first present an analytical approach to understanding the dynamical behavior of the measurement, and then demonstrate this behavior experimentally.

II. The Princeton Benchmark MPDT

The Princeton Full-Scale Benchmark MPDT (FSBT) system used in this study has operated since 1983, and has been used in extensive studies of thruster performance,[2,3] electrode erosion,[10] and plasma properties. The dimensions of the thruster are shown in Fig. 1. For the experiments in this paper, the thruster was fed with argon propellant at a rate of 4.5 g/s, equally split between the cathode annulus and the outer ring of 12 holes shown in the figure. The cathode is Elkonite, the anode copper, and the insulating surfaces Pyrex and boron nitride.

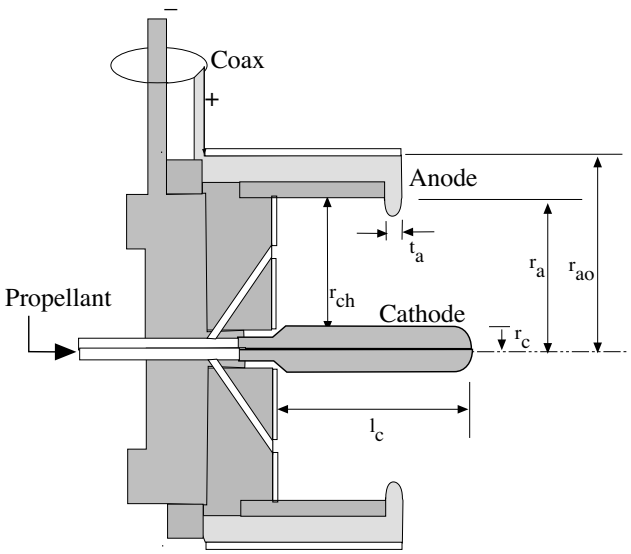

Figure 1. The Princeton Benchmark MPDT. $r_c = 0.95$ **cm,** $r_a = 5.1$ **cm,** $r_{ao} = 9.3$ **cm,** $r_{ch} = 6.4$ **cm,** $t_a = 0.95$ **cm, and** $l_c = 10$ **cm.**

The FSBT is operated in quasi-steady fashion, using a pulse of current supplied by a pulse-forming network (PFN) with a 12.9 mF total capacitance and 14.9 μH total inductance. This PFN supplies 1 ms flat-topped pulses of current up to 25 kA. A stainless steel ballast resistor matches the impedance of the thruster to that of the bank, preventing the current from ringing during the pulse. An air-fed gas switch holds off the full PFN voltage from dropping across the thruster until triggered.

The physical locations of the PFN and the thruster are important details that have been overlooked in previous publications. Space constraints generally require that the PFN be housed at some distance from the thruster (in our case, in the laboratory basement). The power connection between the two is made by a length of transmission line, for us about 35 feet of 40 parallel coaxial cables (RG-8). As Sec. III describes, the remote location of the power supply has a significant effect on the measurement of transient electrical

properties, especially the thruster voltage. Understanding and eliminating the effect of the cabling was the primary driver for the diagnostic work described in this paper.

III. MPDT Voltage Measurement

A. Mathematical Prediction of Cabling Resonance

In Sec. II, we pointed out that the long length of coaxial cabling required to connect the PFN to the MPDT can have a significant effect on the measurement of transient MPDT voltage. This effect—a resonance excited by the voltage hash above onset—is a consequence of the inductance and capacitance of the cabling. In this section we use a simple lumped-parameter model to demonstrate how these resonances arise and how they can be eliminated by proper placement of the voltage probe.

We begin by considering the FSBT to be a voltage signal source $V(t)$ whose output we wish to measure. The measurement may be taken anywhere along an attached coaxial line that extends some length ℓ from $V(t)$. The coaxial line is characterized by an inductance and capacitance per unit length, L' and C', so that the total inductance and capacitance of the line is $\ell L'$ and $\ell C'$.

We will restrict the frequency content of $V(t)$ to frequencies sufficiently low that transmission-line effects along the coaxial line may be ignored. [In the FSBT, the highest frequency peak observed in the spectrum of $V(t)$, viewed out to 20 MHz, is ~ 1.5 MHz; our 11 m cable is therefore short enough to make this analysis approximately applicable ($\ell/\lambda = 5.5\%$, where λ is the wavelength of the signal).] In this limit, the line can be considered as a lumped-element system, as represented in Fig. 2. In this figure, the line has been split into two lumped L-C sections: one to represent the portion of the line between $V(t)$ and the voltage measurement, which is taken across C_1, and the other to represent the portion of the line after the measurement. The first portion represents a fraction $\alpha < 1$ of the length of the line, so that

$$\begin{aligned} L_1 &= \alpha \ell L' \\ C_1 &= \alpha \ell C'. \end{aligned} \tag{1}$$

Similar expressions are true for the second portion, with β replacing α, and $\alpha + \beta = 1$.

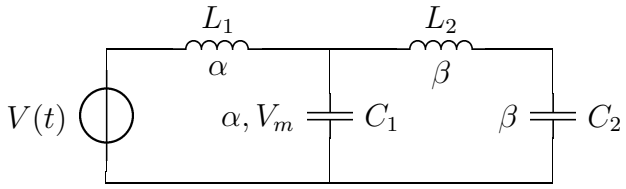

Figure 2. The equivalent circuit of the MPDT and the power supply cabling, showing as lumped components the distributed capacitance and inductance of the cabling before (α) and after (β) the voltage measurement.

It is a straightforward circuit-analysis task to calculate the transfer function relating $V(t)$ to V_m in Laplace space (where the Laplace variable s is related to frequency f by $s = -\imath 2\pi f$),

$$\frac{\widetilde{V}_m}{\widetilde{V}(t)} = \frac{1 + C_2 L_2 s^2}{C_1 C_2 L_1 L_2 s^4 + [(C_1 + C_2)L_1 + C_2 L_2]s^2 + 1}. \tag{2}$$

The transfer function can be generalized using the relations in Eqs. (1) and the nondimensional frequency κ, defined as

$$\kappa \equiv s\ell\sqrt{C'L'}. \tag{3}$$

The result is

$$\frac{\widetilde{V}_m}{\widetilde{V}(t)} = \frac{1 + \beta^2\kappa^2}{\alpha^2\beta^2\kappa^4 + (\beta^2 + \alpha)\kappa^2 + 1}. \tag{4}$$

In Eq. (4), varying the value of $0 \le \alpha \le 1$ corresponds to moving the voltage measurement along the coaxial line from the location of $V(t)$ to a point ℓ distant from $V(t)$. Figure 3 shows the gain of the transfer function in Eq. (4) for several values of α. For each value of $\alpha \neq 0, 1$, there are two resonances, the high-frequency corresponding to the L_1C_1 resonance, and the low-frequency corresponding to the $(L_1 + L_2)C_2$ resonance. The two resonances merge at $\alpha = 1$, as there are no longer separate L_1 and C_1 and L_2 and

C_2. We will concern ourselves with the lower resonance, as it is the more likely of the two to appear in experiments. This resonance occurs near (or perfectly at, for $\alpha = 1$) a normalized frequency of unity, which corresponds dimensionally to $\omega^2 = 1/(L'C')\ell^2$. Its magnitude increases with α, and acts to significantly distort the measurement of $V(t)$ at values of α as low as 0.1.

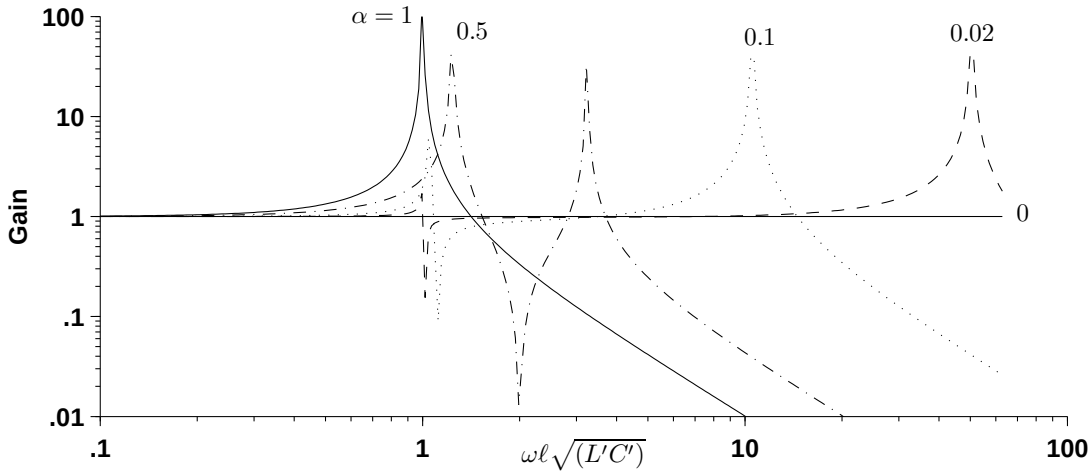

Figure 3. The magnitude of the transfer function of Eq. (4) for several values of α. The smaller the value of α, the less significant the resonance—but only for very small α can it be neglected.

These insights from Eq. (4) are useful to illustrate the effect of a voltage measurement located at some distance from $V(t)$. In practice, however, there is rarely a simple line leading from $V(t)$ with a single value of L' and C'; rather, as in the case of the FSBT, the power supply line may consist of the thruster mount, switching, vacuum feedthroughs, and so on. In such cases, it is more useful to turn to Eq. (2) and lump into L_1 and C_1 and L_2 and C_2 the contributions of the various parts of the supply line before and after the measurement. Rough estimates of these values for several parts of the Princeton Benchmark setup, good to 20%, are shown in Table 1, calculated using the part geometries and standard formulae.[9] The resonant frequency calculated using these values is ≈ 2 MHz, close to the experimentally observed value of 1.3 MHz. The difference is made up by the inductance and capacitance of connections, feedthroughs, and switching apparatus whose values are not simply estimated.

Table 1. Values of inductance and capacitance for parts of the Princeton FSBT power system.

Component	L (μH)	C (pF)
Thruster	229×10^{-6}	83
Stand Arm	0.133	339
Coaxial Line	2.3	878
Ballast Resistor	0.74	683

We may comment here that additional values of L and C may be added as extra rungs on the ladder network of Fig. 2 to represent the PFN. A single extra value of each, L_3 and C_3, will add another resonance to the two already discussed, and alter the magnitudes of those two. We will note, however, that for the values of L_3 and C_3 represented by a PFN such as ours, the frequency of the added resonance is far below those just discussed, and the larger L_3 and C_3, the less significant the effect on the magnitudes of the resonances. A single station in our PFN has $C = 644$ μF and $L = 2.7$ μH, which places the new resonance at 2.6 kHz, and changes very little the magnitude of the cabling resonance. The influence of the PFN on the voltage measurement distortion can therefore be ignored.

A final comment is appropriate here, in the discussion of the frequency response of the power supply cabling. We may easily calculate the current driven by $V(t)$ in the cabling using the same straightforward

Laplace transform mathematics as produced Eqs. (2) and (4). The result is

$$\frac{Z_o\widetilde{I}}{\widetilde{V}_{in}} = \frac{\kappa\left(\alpha\beta^3\kappa^2+1\right)}{\alpha^2\beta^2\kappa^4+(1-\alpha\beta)\kappa^2+1}. \tag{5}$$

$Z_o = \sqrt{L'/C'}$ is the characteristic impedance of the cabling. In the calculation of the current, there is little reason to split the cabling into two sections, and it is immaterial whether $\alpha = 0$ or $\beta = 0$. The current is therefore represented by

$$\frac{Z_o\widetilde{I}}{\widetilde{V}_{in}} = \frac{\kappa}{\kappa^2+1}. \tag{6}$$

We will discuss the implications of Eq. (6) in Sec. IV in the context of MPDT current measurements.

B. Experimental Demonstration and Elimination of Cable Resonance

Based on the discussion of Sec. III.A, the voltage measurement across the FSBT must be made as closely as possible to the signal source, which is the thruster electrodes. We chose the new location of our voltage measurement to be 7.5 cm behind the upstream end of the thrust chamber, at the axial location of the "Coax" connection labeled in Fig. 1; this is sufficiently close to eliminate most, but not all, of the distorting effects of the resonance in the power supply lines. We also make the measurement simultaneously at the traditional location[3] at the power feedthrough just outside the vacuum tank, at a distance of about 1 m from the thruster. This enables us to make a comparison between the two measurements.

We make the voltage measurements with a commercial Tektronix P5210 100/1000x voltage probe. This probe measures differential mode voltages up to 4400 V with a bandwidth of 50 MHz; both parameters are well above those of nominal FSBT operation. No special preparations are needed to make the measurement at the traditional location ("outside measurement"). To make the measurement at the new location ("inside measurement"), we exposed the cathode-potential inner FSBT structure by drilling a 1/2 inch hole through the thruster body, which is at anode potential, and installed connections on both surfaces to accept the voltage probe leads.

Rather than bring thruster potential outside the vacuum tank, we place the voltage probe for the inside measurement inside the vacuum. Tektronix does not guarantee the vacuum compatibility of its voltage probes, but we have experienced no detrimental effects while using the P5210 and its associated power supply 1103 at pressures down to 6×10^{-5} Torr for extended periods.

We show, in Fig. 4, a comparison of the inside voltage measurement with the outside voltage measurement, for the case of the FSBT firing at 22 kA with 4.5 g/s argon propellant feed. This is a condition well above the onset current (14 kA), and significant voltage hash appears on both traces. However, the most prominent feature on the outside measurement is a large-amplitude sinusoidal oscillation around a mean of 350 V with a frequency of 1.3 MHz, whereas what appears most prominently on the inside measurement is a series of voltage spikes rising several hundred volts from a 350 V baseline, each lasting several μs. Different conclusions about the physical nature of the voltage hash would be drawn if each of these measurements were inspected separately—but from the discussion of Sec. III.A, the correct interpretation of the voltage hash shape must come from the inside measurement.

Power spectra of the two measurements are shown in Fig. 5. The two power spectra are quite similar from DC through several hundred kHz, but the outer measurement begins to rise to its resonance around 700 kHz. The peak of the resonance on the inside measurement is six times smaller than that of the outside measurement. Each of these observations would be expected from the results displayed in Fig. 3. Because the resonance is so large and broad, attempts to filter the 1.3 MHz oscillation from the outside measurement affect frequencies well down into the hundreds of kHz, which leaves the filtered waveform bearing only a loose resemblance to the true waveform.

The examples presented in this section demonstrate the importance of locating the voltage measurement as close as possible to the thruster in MPDT experiments in which voltage oscillations are of interest. In some cases it may not be necessary to place the measurement so carefully—if, for example, the power transmission line is not so long that its resonant frequency appears near the frequencies of interest. In general, though, ignoring the distorting effects of the thruster power supply can significantly change the conclusions drawn from the voltage data.

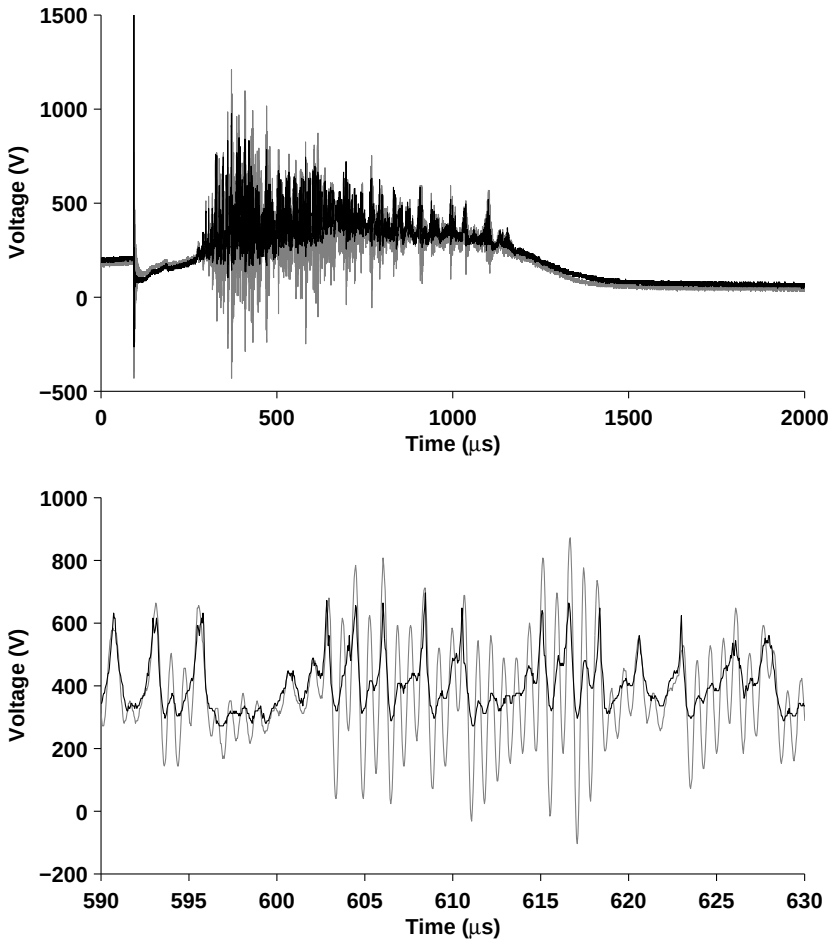

Figure 4. Plots of FSBT voltage for a quasi-steady firing at 22 kA, 4.5 g/s argon. In both the full (upper) and expanded (lower) views, the grey trace is the "outside" measurement and the black trace the "inside" measurement. The effect of the resonance at 1.3 MHz is to distort the signal sufficiently that the true structure is unidentifiable.

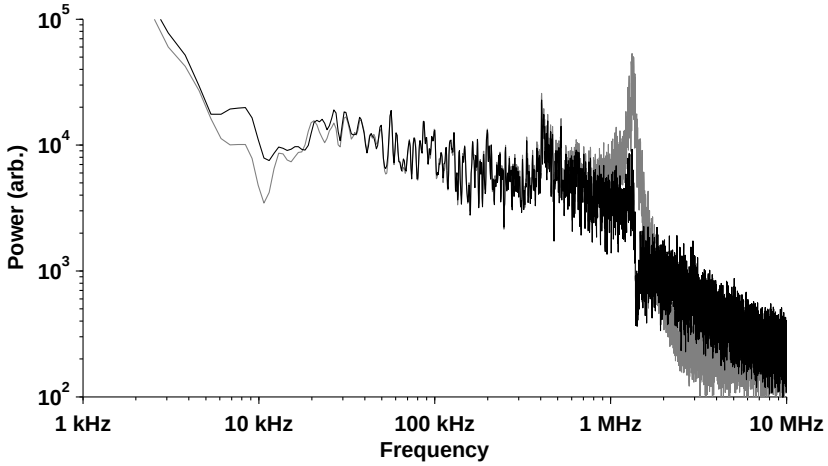

Figure 5. The power spectra of the quasi-steady portions of the voltage traces in Fig. 4. They are largely identical until the resonance takes effect.

IV. MPDT Current Measurement

A. PCB Rogowski Coils for Fast Current Measurement

In this section, we describe a Rogowski coil that we specifically designed and manufactured to measure the current in pulsed MPDTs such as the FSBT. Having seen the influence of the power supply cabling on the voltage measurement, we desire to understand any such influence on the current measurement by measuring at the location that best contributes to our understanding of thruster physics: at the thruster electrodes. In particular, we wish to be able to see any significant fluctuations in the thruster current: our understanding of the onset phenomenon partly hinges on whether or not voltage hash is accompanied by a constant or non-constant current.

The best choice of current diagnostic to incorporate *a posteriori* into the FSBT setup is the Rogowski coil, which can be made smaller than a ferrite-core transformer, and is not prone to core saturation at the high currents being measured. Recently,[5,6,11] a method of mass-producing identical Rogowski coils of varying sizes and sensitivities has been developed based on printed circuit boards (PCBs). In these designs, the coil is produced by connecting printed traces on alternating sides of a silicon board with vias, or plated through-holes. This produces a coil with a rectangular poloidal cross-section, and because the manufacture is based on an automated process, many identical coils can be cheaply produced. This also makes it easy to control the coil's inductance and interturn capacitance, which together work to determine the bandwidth and sensitivity of the ideal measurement. Coil-only bandwidths of 10 MHz or more[5] and very small response to external currents[11] have been reported.

In the remainder of this section, we describe the design and use of a PCB Rogowski coil system. As the design of the coil itself is a topic that has received substantial coverage elsewhere,[5,11] we will not again describe that aspect of the system. We will instead focus on the unique peculiarities encountered when using, as we of necessity do, a coil of small inductance at a location distant from the recording electronics.

B. Analysis of the FSBT Rogowski Coil System

Of the several design parameters we considered in designing the Rogowski coil diagnostic for the FSBT, the most important were: size (the coil must fit into the thruster assembly, where spatial tolerances are tight); mutual inductance (the output of the coil, when presented with large thruster currents, must be large enough to provide a good signal, but small enough to cause no damage to measurement electronics); and bandwidth (it must be good for measuring at least those frequencies that are present in the voltage signals). These design criteria are all met by printing the Rogowski coil on a standard-thickness (1/8") silicon circuit board. We describe the system assembly in Sec. IV.C; in this section, we discuss the expected bandwidth of the current measurement, and in particular the effect of the coil cabling on the relatively low frequency content of the signal.

Because we are, in this setup, only interested in signal frequencies below a few MHz, the 12 feet of cabling leading from the Rogowski coil to the termination in digitizing electronics is far shorter than the wavelengths of interest. The cabling can therefore be treated as a lumped inductance and capacitance (with resistance negligible compared with the termination). In this case, the Rogowski coil system equivalent circuit is shown in Fig. 6, with the cabling elements shown as L_ℓ and C_ℓ. The Rogowski coil itself is shown as a lumped R_c, L_c, and C_c, and the applied voltage source is proportional to the derivative of the current enclosed by the coil:

$$V(t) = M\frac{dI}{dt}(t). \tag{7}$$

The coil parameters are determined by the specified coil geometry, and for our coil—shown photographed in Fig. 8—can be calculated in the ideal case[1] as shown in Table 2. In practice, only small ($< 1\%$) deviations from these values may be expected thanks to strict circuit board printing tolerances.

The small values of L_c and C_c are a consequence of meeting the design criteria of the first paragraph. The value $M = 1.35$ nH means that the typical current rise of our PFN pulse, $\sim 10^8$ A/s, will produce a 100 mV output across the Rogowski coil, and any large, faster transients are unlikely to produce more than 2 V output, which marks the linear range of the electronics mentioned in Sec. IV.C.

The values of L_ℓ and C_ℓ given in Table 2 are calculated for the specific values of the cabling used in our setup: 12 ft of Belden 9452 twisted shielded pair, with published values of inductance and capacitance per foot of 0.18 μH and 30 pF, respectively. An important point to notice is that $L_c \ll L_\ell$ and $C_c \ll C_\ell$, and will be for any practical length of cable. We immediately conclude that the cabling will have a dominant

Table 2. Values of the Rogowski coil equivalent circuit parameters

Parameter	Value
L_c	48.5 nH
C_c	2.66 pF
R_c	0.475 Ω
M	1.35 nH
L_ℓ	2.16 μH
C_ℓ	360 pF

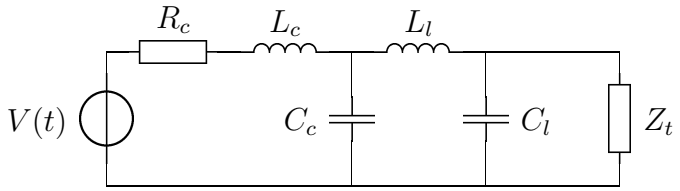

Figure 6. The Rogowski coil system equivalent circuit. $V(t)$ **is the Rogowski output voltage,** R_c, L_c, C_C **the coil parameters, and** L_ℓ, C_ℓ **the cabling parameters, all given in Table 2.** Z_t **is the impedance terminating the cabling.**

effect on the dynamical response of the system, a conclusion that is borne out in an analysis of the transfer function.

The transfer function of this system is, s having the same significance as in Sec. III.A,

$$\begin{aligned}\frac{\widetilde{V}_{Z_t}}{\widetilde{V}(t)} =& Z_t \left\{ Z_t C_c C_\ell L_c L_\ell s^4 + C_c L_\ell (L_c + Z_t C_\ell R_c) s^3 + [Z_t (C_c L_c + C_\ell (L_c + L_\ell)) + C_c L_\ell R_c] s^2 \right. \\ & \left. + [L_c + L_\ell + Z_t R_c (C_c + C_\ell)] s + (R_c + Z_t) \right\}^{-1}. \end{aligned} \tag{8}$$

Equation (8) contains two important insights, which are evident in the curves of Fig. 7. The first we have already stated: the electrical properties of the cabling connecting the Rogowski coil to the termination have a significant effect on the frequency response, the result of $L_c \ll L_\ell$ and $C_c \ll C_\ell$. Curves (a) and (b) show the frequency response of the coil system without and with inclusion of the cabling parameters: it is apparent that cabling lowers the bandwidth of the measurement. The cabling should therefore be made as short as possible, to lower L_ℓ and C_ℓ. In our experiment, 12 ft is the minimum length necessary to move the signal out of the vacuum tank to the digitizing electronics, which could not be moved inside.

The second insight involves the termination impedance Z_t. Without the effect of the cabling, the value of Z_t does not matter until the frequency of the signal becomes very large, when the combination of L_c and Z_t forms a low-pass filter that effectively integrates the signal. With the much larger value of L_ℓ, however, the pole of the low-pass filter formed by L_ℓ and Z_t sits at a much lower frequency and may attenuate frequencies of interest. In response to this, the signal of the coil should, in general, be terminated into a high impedance. (The relevant comparison is between Z_t and $\sqrt{L_\ell / C_\ell}$.) Curve (c) in Fig. 7 shows the response of our system with $Z_t = 10$ Ω; in contrast, curves (a) and (b) are calculated with $Z_t = 56.2$ kΩ.

C. Rogowski Coil Installation and Calibration

We installed the Rogowski coil analyzed in the last section into the FSBT assembly at the axial location labeled "Coax" in Fig. 1. Because in this location the Rogowski coil is surrounded by an assembly floating at cathode potential, the coil is insulated by a G10 housing, whose dielectric strength is sufficient to hold off several thousand volts and whose hardness is sufficient to withstand the pressure required to ensure the cathode makes good electrical contact with the rest of the thruster. The housing is sealed with a silicon RTV. The coil assembly is shown in Fig. 8.

The proximity of the coil to the arc allows the coil and its cabling to pick up a significant amount of electrical noise. We have found it insufficient merely to fit the Rogowski coil with an electrostatic shield

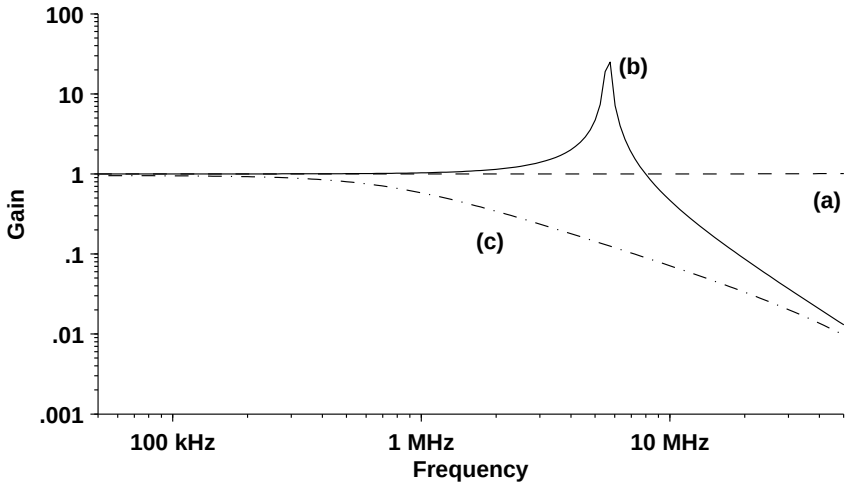

Figure 7. The calculated frequency response of the PCB Rogowski coil (a) alone, terminated into 56 kΩ; (b) with 12 ft of twisted shielded pair cabling terminated into 56 kΩ; and (c) like (b), but terminated into 10 Ω.

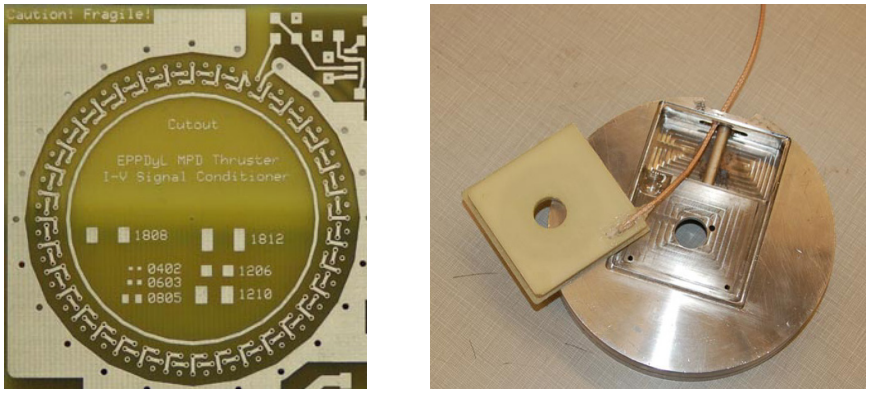

Figure 8. (left) A picture of the printed Rogowski coil. Visible are the top traces (L-shaped) and the return lead through the center of the coil. (right) The enclosed coil at its installation location: the cathode is inserted through the hole in the G10, which aligns with the hole in the steel backpiece.

surrounding the windings at ground potential—such a configuration, in which one end of the coil is grounded to the shield, and the other is brought out on the center conductor of a coaxial cable, allows the signal to be corrupted by a significant amount of common-mode noise. Instead, as pointed out in the previous section, we use twisted shielded pair, with the shield grounded at one end of the line and connected to the Rogowski coil shield at the other, to bring the coil signal to the recording electronics differentially. The signals on the twisted pair are then subtracted by an active balanced/unbalanced signal converter,[13] whose 20 MHz bandwidth is sufficient to pass all frequencies of interest. This balanced signal transmission greatly attenuates common-mode signals, as any noise picked up at the coil or along the cabling is transmitted equally along both conductors and is therefore subtracted out of the final signal.

Because of the just-demonstrated effect of the cabling on the Rogowski coil output, we calibrate the coil only after it is installed into the FSBT. A sinusoidal current with a known amplitude I and frequency ω produces a measured output V_{out} from the coil; using the Fourier transform of Eq. (7), $M = V_{out}/\omega I$. Any amplitude I can be used for the calibration, because the Rogowski coil produces a linear response; however, because M is small, the coil output approaches the measurement resolution of standard oscilloscopes for small I and ω, using available RF power amplifiers. Figure 9 shows the in-situ calibration performed on our setup. Approaching several MHz, the curve begins to rise as the resonance described in the last section is approached; in the low kHz, the value of M begins to rise as well, but due only to difficulty in measuring the low signal output at such low frequencies. Ignoring such low frequencies, and frequencies approaching resonance (which are above our frequency range of interest), the mean value of the calculated mutual inductance is $M = (1.32 \pm .05)$ nH, in favorable comparison with the calculated value $M = 1.35$ nH from Table 2.

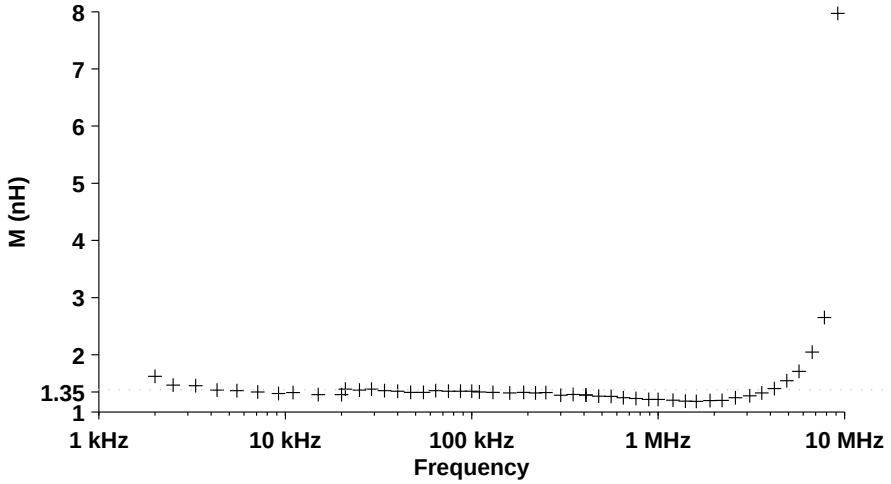

Figure 9. The measured Rogowski coil mutual inductance over the range of frequencies encountered in the FSBT. Uncertainties in the measurement are represented by the vertical size of the data markers.

D. Experimental Use of Rogowski Coil System

The small value of mutual inductance M produces a convenient output voltage in response to the large currents driving the FSBT. It does not, however, make easy a comparison between its response to a known driving current and that of a calibrated current measurement. To accomplish this comparison, we use the FSBT itself at a relatively low current—10 kA, below the onset current—to provide a test pulse. This enables a comparison between the performance of the Rogowski coil system just described and a commercial current transformer, in this case a Pearson model 301X.

To simplify the setup, we digitize the output of the Rogowski coil and numerically integrate *a posteriori*. Figure 10 shows a comparison between the current as measured by our Rogowski coil and that of the Pearson transformer. The favorable agreement provides assurance that the coil behaves as anticipated.

We may get a feel for how the MPDT voltage hash during onset will affect the current through the thruster by looking back at Eq. (6), which relates the current driven through the cabling due to $V(t)$ to the magnitude of $V(t)$ as a function of frequency. A plot of this function is shown in Fig. 11, which manifests

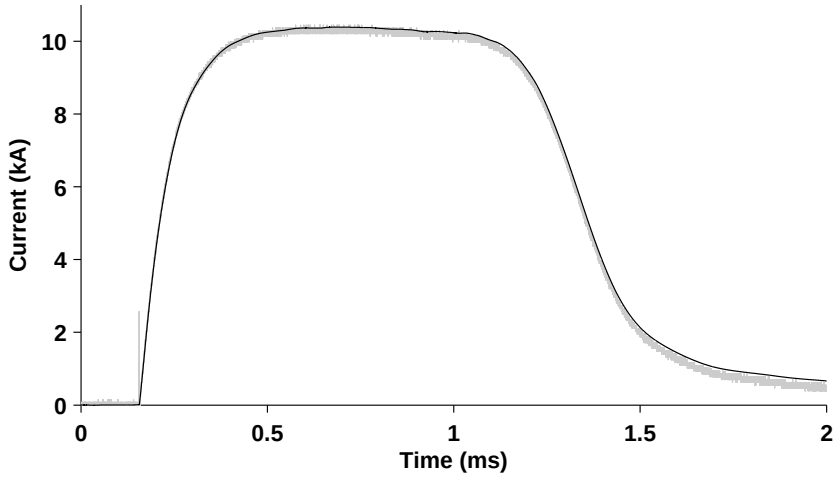

Figure 10. A comparison of the Rogowski coil output (black trace) and that of a commercial current transformer (gray trace) for a 10 kA test pulse.

a sharp resonance around the resonant frequency $\omega = 1/\ell\sqrt{L'C'}$ of the cabling. This resonance indicates that the cabling presents a much lower impedance to current flow at this frequency than at others, so that currents at the resonant frequency will be dominant in the signal.

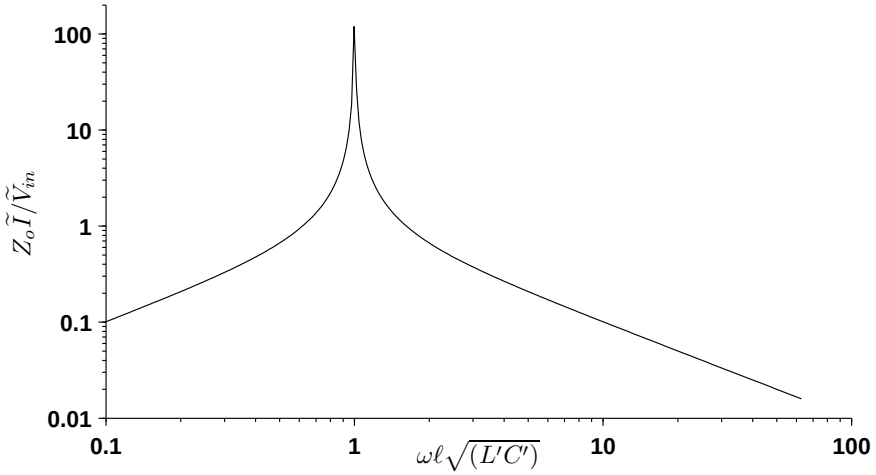

Figure 11. The frequency-dependent current response of the power supply cabling to $V(t)$. The resonance at $\kappa = \omega\ell\sqrt{L'C'}$ corresponds to the resonance in the voltage transfer function shown in Fig. 3.

Since Z_o of our cabling is 50 Ω, a 1 V signal applied by $V(t)$ at the resonance (which for the FSBT is 1.3 MHz) will produce a $\sim$ 2.4 A current. The voltage hash, as shown in Fig. 4, can reach magnitudes as high as 500 V, but with a fundamental frequency significantly off of the resonance: Fig. 5 shows a fundamental peak at $\sim$ 500 kHz. A 500 V signal at 500 kHz would affect the current through the thruster by $\sim$ 5 A, an amount too small to be noticed. At 1.3 MHz, the current effect would be on the order of 1 kA, but the magnitude of this frequency component in $V(t)$ is much smaller than that of the fundamental. This leads us to expect that the current measurement will show a good deal of relatively low-amplitude oscillation about the mean at 1.3 MHz, and very little variation at other frequencies of interest.

This prediction is borne out in the experimental results. Figure 12 shows the voltage and current across and through the FSBT during a firing above onset. The fundamental frequency present in the voltage trace is in the hundreds of kHz, corresponding to the recurrence frequency of the voltage spikes. On the other hand, the dominant frequency in the current trace is 1.3 MHz, reflecting the much lower line impedance

presented to this frequency compared with all others. During even the most pronounced of the voltage hash, the current variation is only hundreds of Amperes, small compared to the mean current. We conclude that though the effect of the power supply line is manifest in the current trace, it is not of a sufficient magnitude to cause concern in the interpretation of onset phenomena.

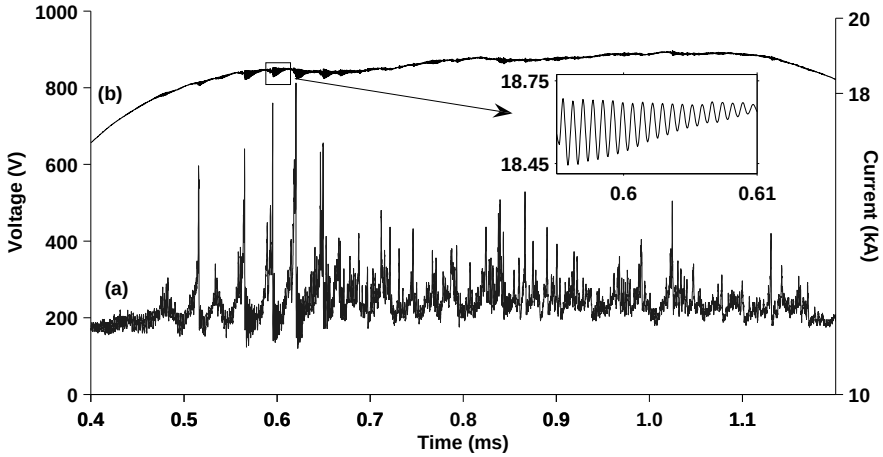

Figure 12. The voltage (a) and current (b) across and through the FSBT during a firing above onset (~ 19 kA, 4.5 g/s argon). The spikes in the thruster voltage set off current oscillations with an amplitude of hundreds of Amperes and a frequency of 1.3 MHz, but the forms of the voltage spikes themselves are not reproduced in the current trace (inset).

V. Conclusion

The proper measurement of transient properties, particularly the thruster voltage, is essential in studies of the onset phenomenon in MPDTs, where the fluctuating quantities are of primary interest. Measurements of fluctuating quantities, however, are subject to corruption by the power supply circuit that drives the MPDT, and care must be taken to recognize and minimize this source of corruption.

In order to accomplish this, we have discussed the manner in which a resonance in the transfer function of the power supply cabling causes an otherwise insignificant frequency component in the fluctuating voltage to become prominent. We first derived the resonance analytically, showed how its magnitude changed in response to the physical location of the voltage measurement, and then demonstrated this dependence experimentally. We also showed, both analytically and experimentally, the influence of the power supply cabling on the thruster current. We concluded that the response of the voltage measurement to the cabling was sufficient to dramatically alter the physical interpretation of the voltage hash, but that the response of the current measurement was too small to be significant. In the process, we discussed several practical and important issues relating to the physical placement of the voltage measurement, the length of the cabling to which our low-inductance Rogowski coil was attached, and the impedance into which the coil was terminated.

These conclusions make possible a further investigation of the physical nature of the onset phenomenon. In particular, the anode spot hypothesis,[4,12] which regards the fluctuations of the voltage as manifestations of the ignition and extinction of preferential points of current attachment at the anode, is consistent with the shape of the voltage hash measured by our "inside" measurement, but not with the shape of our "outside" measurement. Further analysis of the voltage hash, measured as discussed in this paper, will provide insight into the origin of voltage hash, which could not have been gained before the influence of the power supply was well understood.

Acknowledgments

The authors would like to thank the National Defense Science and Engineering Graduate Fellowship program and the Princeton Program in Plasma Science and Technology for support at various points during this work. We would also like to acknowledge the invaluable technical assistance of Bob Sorenson.

References

[1]Marta Argueso, Guillermo Robles, and Javier Sanz. Implementation of a rogowski coil for the measurement of partial discharges. *Review of Scientific Instruments*, 76(6):065107, 2005.

[2]R. L. Burton, K. E. Clark, and R. G. Jahn. Measured performance of a multi-megawatt MPD thruster. *Journal of Spacecraft and Rockets*, 20(3):299–304, 1983.

[3]E.Y. Choueiri and J.K. Ziemer. Quasi-steady magnetoplasmadynamic thruster performance database. *Journal of Propulsion and Power*, 17(4):520–529, Sept/Oct 2001.

[4]Kevin D. Diamant, Edgar Y. Choueiri, and Robert G. Jahn. Spot mode transition and the anode fall of pulsed magnetoplasmadynamic thrusters. *Journal of Propulsion and Power*, 14(6):1036–1042, November-December 1998.

[5]Nicolas Karrer and Patrick Hofer-Noser. Pcb rogowski coils for high di/dt current measurement. In *IEEE 31st Power Electronics Specialists Conference*, volume 3, pages 1296–1301, June 2000.

[6]Ljubomir A. Kojovic. Pcb rogowski coil designs and performances for novel protective relaying. In *Power Engineering Society General Meeting*, volume 2, page 614. IEEE, July 2003.

[7]K. Kuriki and H. Iida. Spectrum analysis of instabilities in MPD arcjet. *International Electric Propulsion Conference*, (IEPC84-28), 1984.

[8]H. L. Kurtz, M. Auweter-Kurtz, W. D. Merke, and H. O. Schrade. Experimental mpd thruster investigations. *19th International Electric Propulsion Conference*, (AIAA-87-1019), 1987.

[9]Richard E. Matick. *Transmission lines for digital and communication networks; an introduction to transmission lines, high-frequency and high-speed pulse characteristics and applications*. McGraw-Hill, New York, 1969.

[10]J. E. Polk. Measurement of mpd thruster erosion using surface layer activation. *Journal of Propulsion and Power*, 3(1):33–38, January 1987.

[11]Chen Qing, Li Hong-bin, Zhang Ming-ming, and Liu Yan-bin. Design and characteristics of two rogowski coils based on printed circuit board. *IEEE Transactions on Instrumentation and Measurement*, 55(3):939–943, June 2006.

[12]Luke Uribarri and E. Y. Choueiri. The onset of voltage hash and its relationship to anode spots in magnetoplasmadynamic thrusters. *International Electric Propulsion Conference*, (IEPC-2005-084), 2005.

[13]R. C. Webber. Tutorial on beam current monitoring. In *American Institute of Physics Conference Series*, volume 546, pages 83–104, November 2000.